ARTICLES

Journal of Semiconductors
(2022) 43, 072501
doi: 10.1088/1674-4926/43/7/072501

$(Ca,K)(Zn,Mn)_2As_2$: Ferromagnetic semiconductor induced by decoupled charge and spin doping in $CaZn_2As_2$

Jinou Dong[1], Xueqin Zhao[1], Licheng Fu[1], Yilun Gu[1], Rufei Zhang[1], Qiaolin Yang[1], Lingfeng Xie[1], and Fanlong Ning[1, 2, 3, †]

[1]Zhejiang Province Key Laboratory of Quantum Technology and Device and Department of Physics, Zhejiang University, Hangzhou 310027, China

[2]Collaborative Innovation Center of Advanced Microstructures, Nanjing University, Nanjing 210093, China

[3]State Key Laboratory of Silicon Materials, Zhejiang University, Hangzhou 310027, China

Abstract: We have successfully synthesized a novel diluted magnetic semiconductor $(Ca_{1-2x}K_{2x})(Zn_{1-x}Mn_x)_2As_2$ with decoupled charge and spin doping. The substitutions of (Ca^{2+}, K^+) and (Zn^{2+}, Mn^{2+}) in the parent compound $CaZn_2As_2$ (space group $P\bar{3}m1$ (No. 164)) introduce carriers and magnetic moments, respectively. Doping only Mn into $CaZn_2As_2$ does not induce any type of long range magnetic ordering. The ferromagnetic ordering arise can only when K^+ and Mn^{2+} are simultaneously doped. The resulted maximum Curie temperature reaches ~7 K, and the corresponding coercive field is ~60 Oe. The transport measurements confirm that samples with K and Mn co-doping still behave like a semiconductor.

Key words: $CaZn_2As_2$; ferromagnetic ordering; Curie temperature; diluted magnetic semiconductor

Citation: J O Dong, X Q Zhao, L C Fu, Y L Gu, R F Zhang, Q L Yang, L F Xie, and F L Ning, $(Ca,K)(Zn,Mn)_2As_2$: Ferromagnetic semiconductor induced by decoupled charge and spin doping in $CaZn_2As_2$[J]. *J. Semicond.*, 2022, 43(7), 072501. https://doi.org/10.1088/1674-4926/43/7/072501

1. Introduction

Diluted magnetic semiconductors (DMSs) have become a focus of research due to their potential application as spintronic devices[1–8]. Scientists started to study the optical and electrical properties of Mn doped GaAs in the 1960s. To observe magnetic interactions in diluted magnetic systems, the atomic concentrations of magnetic elements must be at least a few percentage[9]. However, the chemical solubility of magnetic elements in bulk III–V semiconductors is extremely low (~0.01%), and no ferromagnetic orders have been formed. With the development of low temperature molecular beam epitaxy (LT-MBE) technology, (Ga,Mn)As epitaxial films with Mn concentrations up to several percentage have been successfully fabricated on GaAs substrates[3, 4, 10–13]. This breakthrough became a milestone in the research line of magnetic semiconductors. Through years of unremitting efforts, the Curie temperature T_C of (Ga,Mn)As film reached ~200 K when the doping concentration of Mn is ~12%[14]. However, this temperature is still lower than the room temperature that is required by practical applications. Dielt *et al.* calculated that the Curie temperature of some semiconductors could be raised to above room temperature when Mn doping contents and hole concentrations reached a certain level[15]. Therefore, mainstream research is still searching for DMS materials that can achieve higher T_C.

In the past decade, a series of bulk form DMSs have emerged that have similar crystal structure as that of iron-based superconductors[16]. We therefore classify them as 111-type, 122-type, 1111-type DMSs, etc.[17–22]. Among these newly discovered bulk form DMSs, the 122-type DMS system is one of the most important families[23]. In general, the 122-type compounds can crystallize into two different structures. The first is the tetragonal $ThCr_2Si_2$ structure, such as the p-type $(Ba,K)(Zn,Mn)_2As_2$[17, 24] and the n-type $Ba(Zn,Co)_2As_2$[25]. $(Ba,K)(Zn,Mn)_2As_2$ exhibits high Curie temperature (T_C ~180 K). By further optimizing the preparation conditions of the polycrystalline samples, researchers finally succeeded in increasing the Curie temperature T_C to ~230 K, which exceeds the T_C record of (Ga,Mn)As. For the purpose of making p–n junctions, an n-type DMS $Ba(Zn,Co)_2As_2$ with the highest T_C ~ 45 K has also been successfully synthesized. Both $(Ba,K)(Zn,Mn)_2As_2$ and $Ba(Zn,Co)_2As_2$ provide valuable references for studying the origin of ferromagneticsim in DMS systems. The second is the hexagonal $CaAl_2Si_2$ structure, such as $(Ca,Na)(Zn,Mn)_2Sb_2$[26], which has been reported as T_C ~ 10 K and H_C ~ 245 Oe recently. In these DMSs, spins and carriers are introduced by the substitutions of Mn^{2+} for Zn^{2+} and substitutions of atoms with lower valences for atoms with higher valences, respectively. This doping pattern makes it possible to control carriers and spins densities separately, and explore their individual effects on the formation of long-range ferromagnetic ordering.

In this paper, we report the successful synthesis of a new 122-type DMS $(Ca_{1-2x}K_{2x})(Zn_{1-x}Mn_x)_2As_2$ with hexagonal structure, which are further characterized by structural, magnetic and transport measurements. Hole carriers and local spins are introduced by (Ca^{2+},K^+) and (Zn^{2+},Mn^{2+}) substitutions in parent semiconductor $CaZn_2As_2$, respectively. After the optimization of carriers and spins densities, ferromagnet-

Correspondence to: F L Ning, ningfl@zju.edu.cn
Received 14 JANUARY 2022; Revised 26 FEBRUARY 2022.

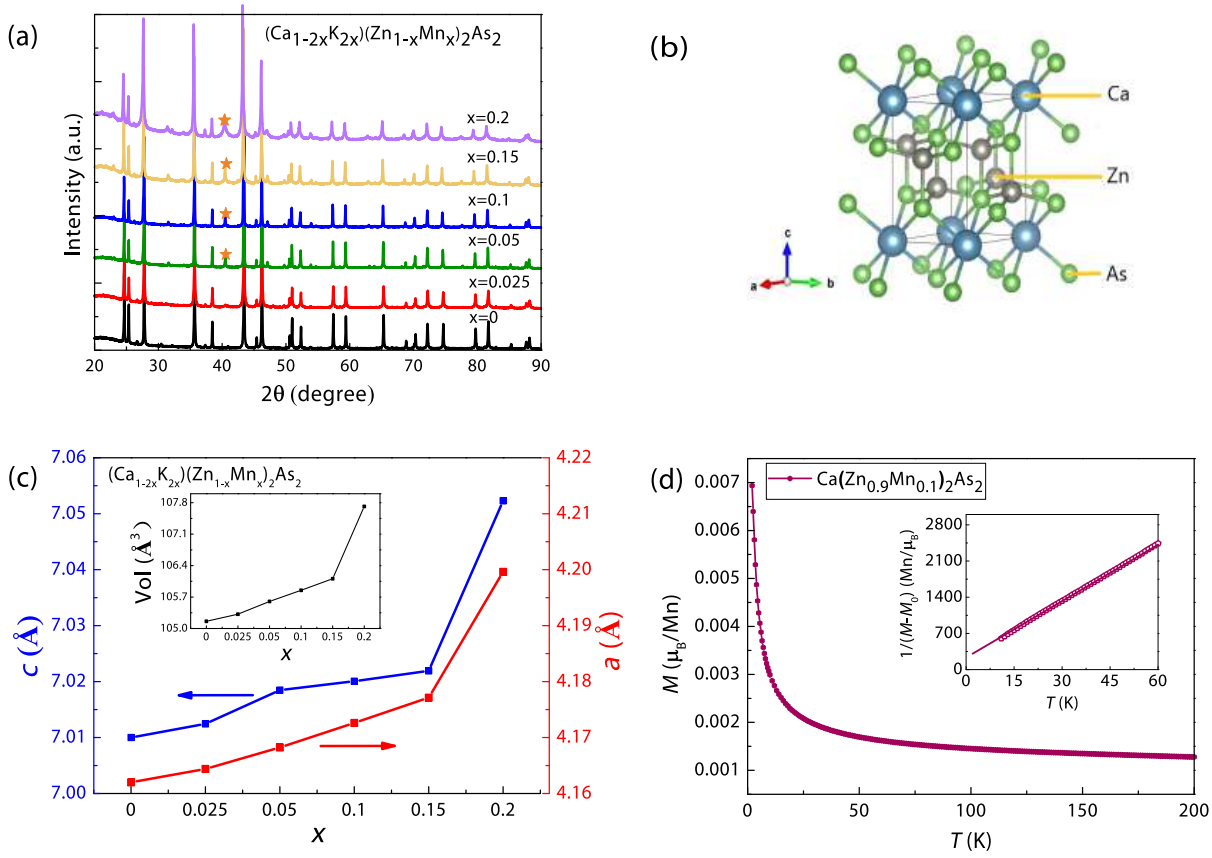

Fig. 1. (Color online) (a) The X-ray diffraction patterns for $(Ca_{1-2x}K_{2x})(Zn_{1-x}Mn_x)_2As_2$ (x = 0, 0.025, 0.05, 0.1, 0.15, 0.2). Star marks the impurities of KZn_4As_3. (b) The crystal structure of $CaZn_2As_2$. (c) The lattice parameters a and c of $(Ca_{1-2x}K_{2x})(Zn_{1-x}Mn_x)_2As_2$ (x = 0, 0.025, 0.05, 0.1, 0.15, 0.2). Inset is the volume of $(Ca_{1-2x}K_{2x})(Zn_{1-x}Mn_x)_2As_2$ (x = 0, 0.025, 0.05, 0.1, 0.15, 0.2). (The standard data are used for x = 0.) (d) The relation of temperature dependent magnetization of $Ca(Zn_{0.9}Mn_{0.1})_2As_2$ measured in the field cooling under 100 Oe. Inset is the plot of $1/(M - M_0)$ versus temperature. The data are marked by hollow dots and the fitting result is plotted by a straight line.

ic ordering with maximum T_C ~ 7 K has been achieved. A clear hysteresis loop can be observed when the doping level is above ~2.5 % and the maximum coercive force H_c is ~ 60 Oe. When K and Mn are co-doped, the resistivity exhibits semiconducting behavior.

2. Experiments

The polycrystalline samples of $(Ca_{1-2x}K_{2x})(Zn_{1-x}Mn_x)_2As_2$ were synthesized via the solid-state reaction of Ca, K, Zn, Mn, and As elements. All of the original elements (99.9 % or higher purity) are stored and handled in an argon filled glove box (the percentage of O_2 < 0.1 ppm and the percentage of H_2O < 0.1 ppm). According to the nominal composition of $(Ca_{1-2x}K_{2x})(Zn_{1-x}Mn_x)_2As_2$, the ingredients were mixed and heated at 200 °C for 10 h in evacuated silica tubes, followed by 1000 min at 700 °C. After natural cooling, we grounded, pelletized, and sealed the products in evacuated silica tubes and heated them again at 700 °C for another 30 h. Excess amounts of Ca (1%) and K (10%) were added to compensate the thermal volatilization. In the powder X-ray diffraction (XRD) measurement, we use X-ray diffractometer (Model EMPRYREAN) with monochromatic Cu $K_{\alpha 1}$ radiation to characterize the crystal structure at room temperature. The DC magnetization measurements were performed on a Quantum Design Magnetic Property Measurement System (MPMS-3). We used the typical four-probe method to measure the electrical resistivity of all of the pellet samples.

3. Results and discussion

In Fig. 1(a), we show the X-ray diffraction patterns for $(Ca_{1-2x}K_{2x})(Zn_{1-x}Mn_x)_2As_2$ ($0 \leqslant x \leqslant 0.2$). All of the detected peaks can be indexed by a hexagonal $CaAl_2Si_2$ structure, which infers that the specimens are isostructural to the parent semiconductor $CaZn_2As_2$ with the space group $P\bar{3}m1$ (No. 164), whose crystal structure is shown in Fig. 1(b). Few impurities, KZn_4As_3[27], can be observed and are marked by stars. These impurities are non-magnetic, and would have no influence on the discussion of the ferromagnetism in the following. We show the lattice parameters obtained from the Rietveld refinement in Fig. 1(c). We can see that the lattice parameters and the volume of the $(Ca_{1-2x}K_{2x})(Zn_{1-x}Mn_x)_2As_2$ unit cell ($0 \leqslant x \leqslant 0.2$) monotonically increase. Since the ionic radius of both K ion and Mn ion are larger than that of Ca ion and Zn ion, this clearly demonstrates the successful chemical doping of K and Mn. In Fig. 1(d), we plot the temperature dependent magnetization of $Ca(Zn_{0.9}Mn_{0.1})_2As_2$ at 100 Oe. The paramagnetic behavior demonstrates that the ferromagnetic ordering does not appear when only Mn atoms are doped. This characteristic is consistent with other DMSs reported before, such as 1111-type and 122-type DMSs[17, 21]. Moreover, the $1/(M - M_0)$ versus temperature curve is a straight line that intersects the $-x$ axis. The Weiss temperature is negative, which suggests that antiferromagnetic interaction dominates for $Ca(Zn_{0.9}Mn_{0.1})_2As_2$.

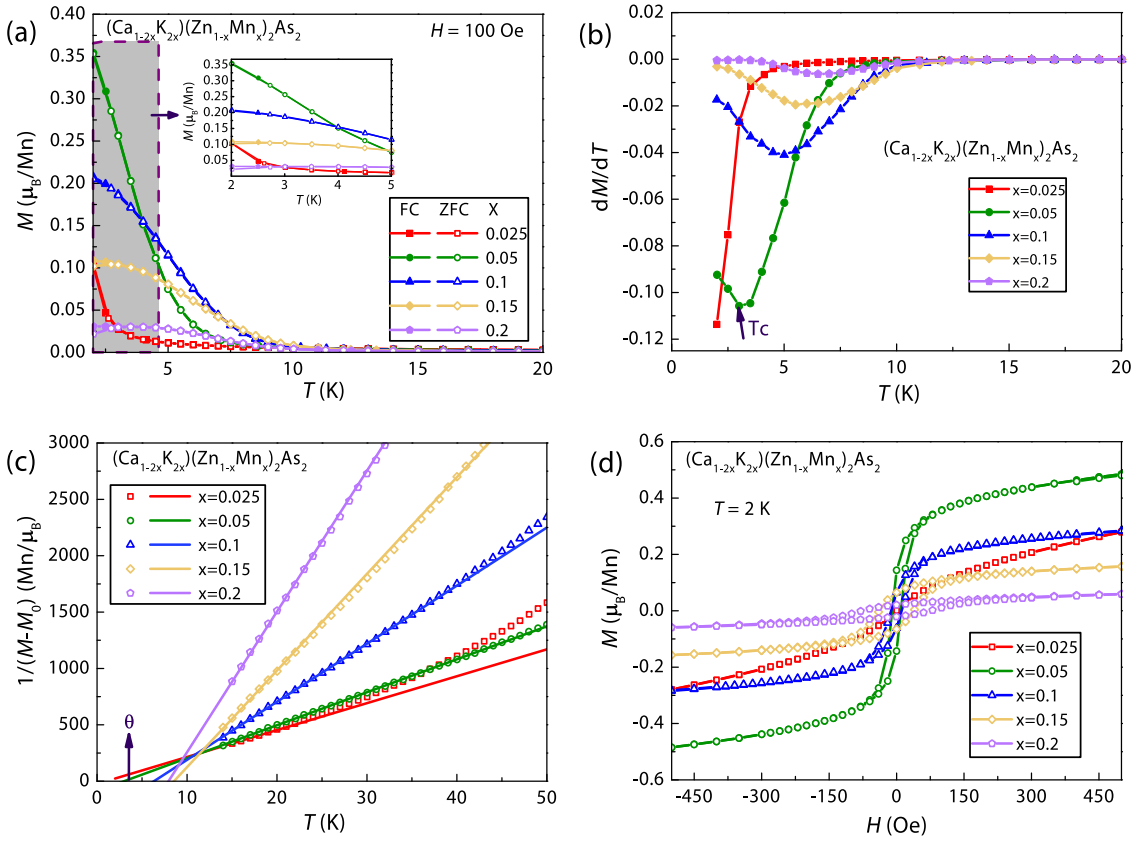

Fig. 2. (Color online) (a) The dependence between temperature and DC magnetization for $(Ca_{1-2x}K_{2x})(Zn_{1-x}Mn_x)_2As_2$ (x = 0.025, 0.05, 0.1, 0.15, 0.2) measured in zero field cooling (ZFC) and field cooling (FC) condition under 100 Oe external field. (b) The first derivative of magnetization versus temperature for $(Ca_{1-2x}K_{2x})(Zn_{1-x}Mn_x)_2As_2$ (x = 0.025, 0.05, 0.1, 0.15, 0.2). The arrow marks the Curie temperature (T_C) of x = 0.05. (c) The reverse of $M - M_0$ versus temperature for $(Ca_{1-2x}K_{2x})(Zn_{1-x}Mn_x)_2As_2$ (x = 0.025, 0.05, 0.1, 0.15, 0.2). The straight lines are the fitting lines and the hollow symbols are the data dots. The arrow marks the Weiss temperature (θ) of x = 0.05. (d) The iso-thermal magnetic hysteresis measurement for $(Ca_{1-2x}K_{2x})(Zn_{1-x}Mn_x)_2As_2$ (x = 0.025, 0.05, 0.1, 0.15, 0.2) under 2 K.

In Fig. 2(a), we show the temperature dependent DC magnetization for $(Ca_{1-2x}K_{2x})(Zn_{1-x}Mn_x)_2As_2$ (x = 0.025, 0.05, 0.1, 0.15, 0.2) measured in zero field cooling (ZFC) and field cooling (FC) condition under a 100 Oe external field. As we can see, the curve still exhibits the paramagnetic behaviour for x = 0.025, which indicates that ferromagnetic ordering does not exist for x = 0.025. The magnetization increases abruptly below T ~ 20 K when the concentration x is larger than 2.5 %. This implies that the ferromagnetic ordering has formed. Moreover, the higher concentrations x we dope, the higher T_C samples behave, reaching the maximum when x equals to 0.15. According to the first derivative of magnetization versus temperature plotted in Fig. 2(b), we define the minimum value of a curve as T_C (numerically, this minimum value is close to the true ferromagnetic transition temperature). The resulted maximum T_C (~ 7 K) is lower than that of $(Ca,Na)(Zn,Mn)_2As_2$[28] (maximum T_C ~ 33 K), but comparable to the value of ~ 10 K in $(Ca,Na)(Zn,Mn)_2Sb_2$[26]. That is probably because the lattice constants of $(Ca,K)(Zn,Mn)_2As_2$ is larger than those of $(Ca,Na)(Zn,Mn)_2As_2$ but close to the parameters in $(Ca,Na)(Zn,Mn)_2Sb_2$. Furthermore, the same behavior can also been observed in $(Sr,Na)(Zn,Mn)_2As_2$[18] whose lattice constants are smaller but larger than those of $(Ca,K)(Zn,Mn)_2As_2$ and $(Ca,Na)(Zn,Mn)_2As_2$, respectively. Consequently, the maximum T_C of $(Sr,Na)(Zn,Mn)_2As_2$ (~24 K) is between that of $(Ca,K)(Zn,Mn)_2As_2$ (~7 K) and $(Ca,Na)(Zn,Mn)_2As_2$ (~33 K). However, we should mention that the relation phenomenal between the lattice constant and the Curie temperature is not strictly justified between different series of compounds. More experimental and theoretical work need to be done to clarify this. The formula of Curie - Weiss $\chi = C/(T - \theta) + \chi_0$ can be used to fit the magnetization curves above T_C, where θ is the Weiss temperature, C is a constant used to calculate the effective magnetic moment, and χ_0 is a temperature independent term. The reverse of $M - M_0$ versus temperature is shown in Fig. 2(c). Based on the data at the high temperature range, the linear fitting lines intersecting the x axis give us the Weiss temperature θ. Similarly, θ values also reach maximum at x = 0.15.

Table 1. The Curie temperature T_C, the Weiss temperature θ, the effective moment M_{eff} , the saturation moment M_{sat} and the coercive field H_c for $(Ca_{1-2x}K_{2x})(Zn_{1-x}Mn_x)_2As_2$.

x	T_C (K)	θ (K)	M_{eff} (μ_B/Mn)	M_{sat} (μ_B/Mn)	H_c (Oe)
0.05	3	4	3.91	0.47	9
0.1	5	7	2.92	0.28	10
0.15	6	9	2.28	0.15	40
0.2	7	8	1.89	0.06	60

We perform the iso-thermal magnetization measurement at 2 K, and show them in Fig. 2(d). Associated with the DC magnetization results, there are clear hysteresis loops

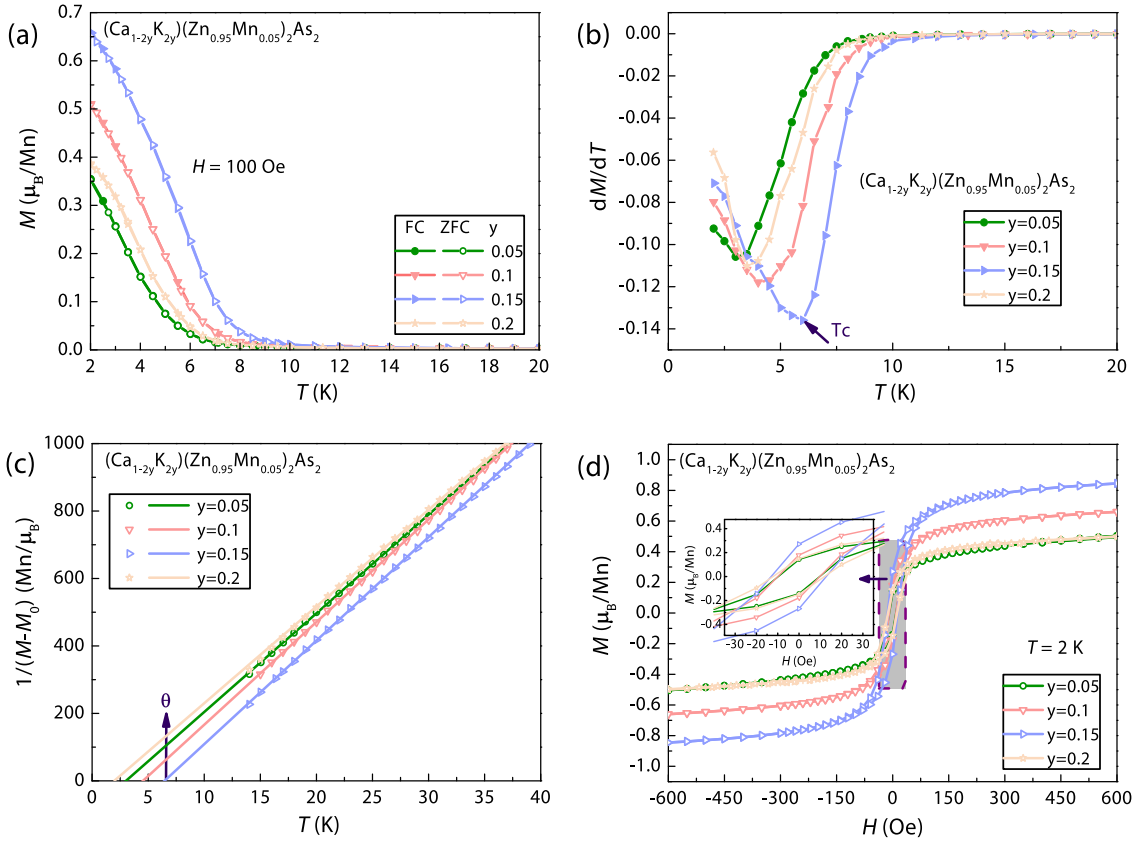

Fig. 3. (Color online) (a) The dependence between temperature and DC magnetization for $(Ca_{1-2y}K_{2y})(Zn_{0.95}Mn_{0.05})_2As_2$ (y = 0.05, 0.1, 0.15, 0.2) measured in zero field cooling (ZFC) and field cooling (FC) condition under 100 Oe external field. (b) The first derivative of magnetization versus temperature for $(Ca_{1-2y}K_{2y})(Zn_{0.95}Mn_{0.05})_2As_2$ (y = 0.05, 0.1, 0.15, 0.2). The arrow marks the Curie temperature (T_C) of y = 0.15. (c) The reverse of $M - M_0$ versus temperature for $(Ca_{1-2y}K_{2y})(Zn_{0.95}Mn_{0.05})_2As_2$ (y = 0.05, 0.1, 0.15, 0.2). The straight lines are the fitting lines and the hollow symbols are the data dots. The arrow marks the Weiss temperature (θ) of y = 0.15. (d) The iso-thermal magnetic hysteresis measurement for $(Ca_{1-2y}K_{2y})(Zn_{0.95}Mn_{0.05})_2As_2$ (y = 0.05, 0.1, 0.15, 0.2) under 2 K.

when doping content x exceeds 2.5%. This implies the formation of the ferromagnetic ordering. In addition, the coercive force H_c has minimum of ~10 Oe for x = 0.05 and increases monotonically with increasing x, rising to the magnitude of ~60 Oe for x = 0.2. Zener's model is effective to study the mechanism of ferromagnetism, and can explain such a change in T_C and H_c[15]. In this model, RKKY-like interactions of Mn spins can be effectively mediated via hole carriers in the valence band, leading to the ferromagnetism. Using nuclear magnetic resonance and muon spin rotation experiments, researchers have investigated and reported similar trends in some DMS systems[29, 30]. The saturation magnetic moment M_{sat} (the value read from $M(H)$ curves) decreases from 0.47 μ_B/Mn for $(Ca_{0.9}K_{0.1})(Zn_{0.95}Mn_{0.05})_2As_2$ to 0.06 μ_B/Mn for $(Ca_{0.6}K_{0.4})(Zn_{0.8}Mn_{0.2})_2As_2$. In general, the M_{sat} of many ferromagnets is ~ 1 μ_B per magnetic atom or larger. Whereas, the value of M_{sat} is only on the order of 0.01 μ_B per magnetic atom or less for typical dilute alloy spin glasses[31–33]. In this system, the minimum of M_{sat} (0.06 μ_B/Mn for x = 0.2) is still larger than that of typical dilute alloy spin glasses. Thus, we recognize the current system as ferromagnets. Simultaneously, we can also get the effective magnetic moment M_{eff} values by fitting to the Curie-Weiss formula, which declines with growing x. The obtained data are tabulated in Table 1. The diminishing behavior of both M_{eff} and M_{sat} probably happens because there is a competition between two interactions in this system: the first is the RKKY interaction mentioned above, and the second is the direct exchange antiferromagnetic coupling caused by Mn atoms at the nearest-neighbor (NN) sites. Similar to our previous work[21], the probability of finding two Mn atoms at NN Zn sites is $P(N; x) = C_N^4 x^N (1 - x)^N$, where N = 1 and x is the doping content. Theoretically, this probability will increase drastically with increasing x, which enhances the direct antiferromagnetic coupling interaction between Mn-Mn pairs. We notice that with this interaction, 100% Mn doped $Ca(Zn_{1-x}Mn_x)_2As_2$, $CaMn_2As_2$, becomes an antiferromagnet with Neel temperature ~ 62 K[34].

Table 2. The Curie temperature T_C, the Weiss temperature θ, the effective moment M_{eff}, the saturation moment M_{sat} and the coercive field H_c for $(Ca_{1-2y}K_{2y})(Zn_{0.95}Mn_{0.05})_2As_2$.

y	T_C (K)	θ (K)	M_{eff} (μ_B/Mn)	M_{sat} (μ_B/Mn)	H_c (Oe)
0.05	3	4	3.91	0.47	10
0.1	4	5	3.83	0.64	10
0.15	6	7	3.81	0.82	10
0.2	3	2	3.94	0.48	10

To verify the impact of carriers on the ferromagnetic ordering, we change the contents of K while fixing the concentration of Mn. In Fig. 3(a), we show the magnetic susceptibility of $(Ca_{1-2y}K_{2y})(Zn_{0.95}Mn_{0.05})_2As_2$ ($0.05 \leqslant y \leqslant 0.2$) measured under B_{ext} ~ 100 Oe. In the same way, we depict the first derivat-

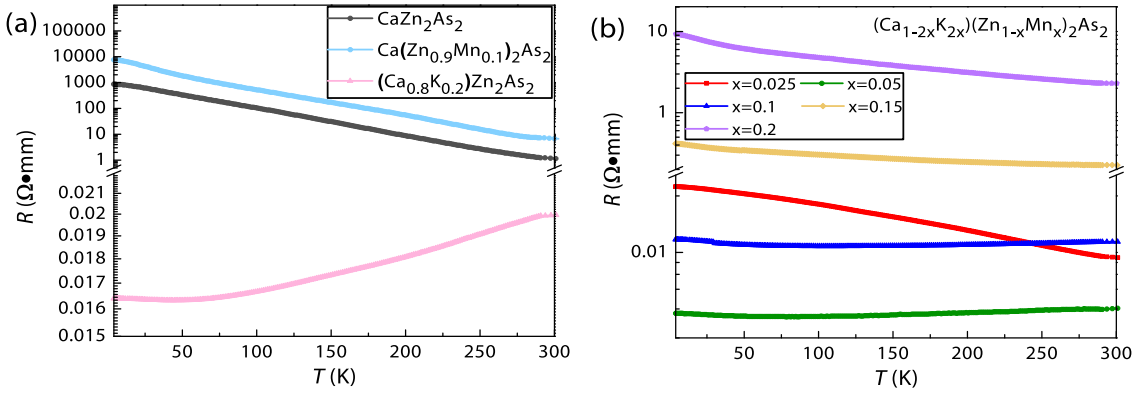

Fig. 4. (Color online) (a) Resistivity for $CaZn_2As_2$, $Ca(Zn_{0.9}Mn_{0.1})_2As_2$ and $(Ca_{0.8}K_{0.2})Zn_2As_2$ in log scale. (b) Resistivity for $(Ca_{1-2x}K_{2x})(Zn_{1-x}Mn_x)_2As_2$ for $x = 0.025$, 0.05, 0.1, 0.15, 0.2 in log scale.

ive of magnetization versus temperature in Fig. 3(b) and the $1/(M - M_0)$ versus temperature in Fig. 3(c). Resembling to the $(Ca_{1-2x}K_{2x})(Zn_{1-x}Mn_x)_2As_2$ mentioned above, T_C and θ monotonically increase with y. Both T_C and θ reach maximum value at $y = 15\%$, indicating the enhancement of ferromagnetism. Furthermore, clear hysteresis loops can be observed at 2 K (in Fig. 3(d)), which presents a soft ferromagnetic behavior with H_c ~10 Oe. Our results indicate that carriers do play a vital role in the formation of ferromagnetic ordering. Nevertheless, for a fixed Mn concentration, the carrier density has to be an ideal level, no more and no less, to optimize the ferromagnetic exchange interaction and the Curie temperature T_C. The data are tabulated in Table 2.

In Fig. 4(a), we show the resistivity measurement results of $CaZn_2As_2$, $Ca(Zn_{0.9}Mn_{0.1})_2As_2$ and $(Ca_{0.8}K_{0.2})Zn_2As_2$, respectively. The results indicate that in terms of transport properties, both $CaZn_2As_2$ and $Ca(Zn_{0.9}Mn_{0.1})_2As_2$ behave as semiconductors, while $(Ca_{0.8}K_{0.2})Zn_2As_2$ behaves like a metal. As we have observed, when a small number of Mn atoms are doped at the Zn sites in $Ca(Zn_{0.9}Mn_{0.1})_2As_2$, the value of the resistivity ρ will increase by an order of magnitude (from ~10^3 to ~10^4 Ω·mm). Nevertheless, if an equal amount of small number of K atoms are doped at the Ca sites, such as in $(Ca_{0.8}K_{0.2})Zn_2As_2$, ρ is drastically reduced by five orders of magnitude (from ~10^3 to ~10^{-2} Ω·mm). The enormous reduction in resistivity demonstrates that doping K atoms will introduce carriers. In Fig. 4(b), the resistivity of $(Ca_{1-2x}K_{2x})(Zn_{1-x}Mn_x)_2As_2$ ($0.025 \leqslant x \leqslant 0.2$) are plotted. At first, the magnitude of resistivity decreases as the concentrations x increases, achieving the minimum value ~0.003 Ω·mm at the doping level of ~5% at 4 K. Above 5% doping, the resistivity starts to increase with x up to 20%. This is presumedly because when more Mn atoms are doped into the Zn sites, the carriers are more likely to be scattered by magnetic fluctuations. Therefore, even though the carrier densities are increasing, the resistivity caused by more Mn atoms is growing. Nevertheless, the resistivity of these co-doped samples is still much lower than that of the parent compound $CaZn_2As_2$. This kind of behavior has also been observed in many DMSs such as $(Sr,K)(Zn,Mn)_2As_2$[35], $(Ca,Na)(Zn,Mn)_2Sb_2$[26], and so on.

4. Summary

In summary, we have successfully synthesized and characterized a novel DMS $(Ca_{1-2x}K_{2x})(Zn_{1-x}Mn_x)_2As_2$ via the structure, magnetic and electronic transport measurements. Doping Mn atoms provides the magnetic moments, and no ferromagnetic long range ordering formed in $Ca(Zn_{0.9}Mn_{0.1})_2As_2$. Ferromagnetism occurs only when K and Mn are co-doped to a certain amount. The resultant maximum T_C and the coercive field H_c is ~ 7 K and ~ 60 Oe, respectively. Meanwhile, the samples with K and Mn co-doping demonstrate the semiconductor characteristic as seen from the electrical transport measurements. This work provides a new option in further research on DMS materials.

Acknowledgements

The work was supported by the Key R&D Program of Zhejiang Province, China (2021C01002) and NSF of China (No. 12074333).

References

[1] Hoefflinger B. ITRS: The International Technology Roadmap for Semiconductors. In: Chips 2020, Springer, 2012, 161
[2] Chappert C, Fert A, Van Dau F N. The emergence of spin electronics in data storage. In: Nanoscience and Technology: A Collection of Reviews from Nature Journals, 2010, 147
[3] Ohno H. Making nonmagnetic semiconductors ferromagnetic. Science, 1998, 281, 951
[4] Dietl T. A ten-year perspective on dilute magnetic semiconductors and oxides. Nat Mater, 2010, 9, 965
[5] Zhao J H, Li Y Q, Xiong P. A pioneer in magnetic semiconductors — Professor Stephan von Molnár. J Semicond, 2021, 42, 010302
[6] Dietl T, Bonanni A, Ohno H. Families of magnetic semiconductors—an overview. J Semicond, 2019, 40, 080301
[7] Hao Y, Wu H Q, Yang Y C, et al. Preface to the special issue on beyond Moore: Resistive switching devices for emerging memory and neuromorphic computing. J Semicond, 2021, 42, 010101
[8] Zhao G Q, Deng Z, Jin C Q. Advances in new generation diluted magnetic semiconductors with independent spin and charge doping. J Semicond, 2019, 40, 081505
[9] Matsukura F, Ohno H, Dietl T. III-V ferromagnetic semiconductors. In: Handbook of Magnetic Materials. Amsterdam: Elsevier, 2002, 1
[10] Ohno H. Ferromagnetic semiconductor heterostructures. J Magn Magn Mater, 2004, 272, 1
[11] Ohno H, Shen A, Matsukura F, et al. (Ga, Mn)As: A new diluted magnetic semiconductor based on GaAs. Appl Phys Lett, 1996, 69, 363
[12] Jungwirth T, Sinova J, Mašek J, et al. Theory of ferromagnetic (III, Mn)V semiconductors. Rev Mod Phys, 2006, 78, 809

[13] Žutić I, Fabian J, Das Sarma S. Spintronics: fundamentals and applications. Rev Mod Phys, 2004, 76, 323
[14] Chen L, Yang X, Yang F H, et al. Enhancing the curie temperature of ferromagnetic semiconductor (Ga, Mn)As to 200 K via nanostructure engineering. Nano Lett, 2011, 11, 2584
[15] Dietl T, Ohno H, Matsukura F, et al. Zener model description of ferromagnetism in zinc-blende magnetic semiconductors. Science, 2000, 287, 1019
[16] Guo S L, Ning F L. Progress of novel diluted ferromagnetic semiconductors with decoupled spin and charge doping: Counterparts of Fe-based superconductors. Chin Phys B, 2018, 27, 097502
[17] Zhao K, Deng Z, Wang X C, et al. New diluted ferromagnetic semiconductor with Curie temperature up to 180 K and isostructural to the '122' iron-based superconductors. Nat Commun, 2013, 4, 1442
[18] Chen B J, Zhao K, Deng Z, et al. (Sr, Na)$(Zn, Mn)_2As_2$: A diluted ferromagnetic semiconductor with the hexagonal $CaAl_2Si_2$ type structure. Phys Rev B, 2014, 90, 155202
[19] Deng Z, Zhao K, Gu B, et al. Diluted ferromagnetic semiconductor Li(Zn, Mn)P with decoupled charge and spin doping. Phys Rev B, 2013, 88, 081203
[20] Deng Z, Jin C Q, Liu Q Q, et al. Li(Zn, Mn)As as a new generation ferromagnet based on a I–II–V semiconductor. Nat Commun, 2011, 2, 422
[21] Ding C, Man H Y, Qin C, et al. $(La_{1-x}Ba_x)(Zn_{1-x}Mn_x)AsO$: A two-dimensional 1111-type diluted magnetic semiconductor in bulk form. Phys Rev B, 2013, 88, 041102
[22] Han W, Zhao K, Wang X C, et al. Diluted ferromagnetic semiconductor (LaCa)(ZnMn)SbO isostructural to "1111" type iron pnictide superconductors. Sci China Phys Mech Astron, 2013, 56, 2026
[23] Gu B, Maekawa S. Diluted magnetic semiconductors with narrow band gaps. Phys Rev B, 2016, 94, 155202
[24] Zhao K, Chen B J, Zhao G Q, et al. Ferromagnetism at 230 K in $(Ba_{0.7}K_{0.3})(Zn_{0.85}Mn_{0.15})_2As_2$ diluted magnetic semiconductor. Chin Sci Bull, 2014, 59, 2524
[25] Guo S L, Man H Y, Wang K, et al. $Ba(Zn, Co)_2As_2$: A diluted ferromagnetic semiconductor with n-type carriers and isostructural to 122 iron-based superconductors. Phys Rev B, 2019, 99, 155201
[26] Gu Y L, Zhang H J, Zhang R F, et al. A novel diluted magnetic semiconductor (Ca, Na)$(Zn, Mn)_2Sb_2$ with decoupled charge and spin dopings. Chin Phys B, 2020, 29, 057507
[27] He H, Tyson C, Bobev S. Eight-coordinated arsenic in the zintl phases $RbCd_4As_3$ and $RbZn_4As_3$: Synthesis and structural characterization. Inorg Chem, 2011, 50, 8375
[28] Zhao K, Chen B J, Deng Z, et al. (Ca, Na)$(Zn, Mn)_2As_2$: A new spin and charge doping decoupled diluted ferromagnetic semiconductor. J Appl Phys, 2014, 116, 163906
[29] Ding C, Qin C, Man H Y, et al. NMR investigation of the diluted magnetic semiconductor $Li(Zn_{1-x}Mn_x)P$ ($x = 0.1$). Phys Rev B, 2013, 88, 041108
[30] Sun F, Li N N, Chen B J, et al. Pressure effect on the magnetism of the diluted magnetic semiconductor $(Ba_{1-x}K_x)(Zn_{1-y}Mn_y)_2As_2$ with independent spin and charge doping. Phys Rev B, 2016, 93, 224403
[31] Nagata S, Keesom P H, Harrison H R. Low-dc-field susceptibility of CuMn spin glass. Phys Rev B, 1979, 19, 1633
[32] Monod P, Préjean J J, Tissier B. Magnetic hysteresis of CuMn in the spin glass state. J Appl Phys, 1979, 50, 7324
[33] Prejean J J, Joliclerc M J, Monod P. Hysteresis in CuMn: The effect of spin orbit scattering on the anisotropy in the spin glass state. J Phys France, 1980, 41, 427
[34] Sangeetha N S, Pandey A, Benson Z A, et al. Strong magnetic correlations to 900 K in single crystals of the trigonal antiferromagnetic insulators $SrMn_2As_2$ and $CaMn_2As_2$. Phys Rev B, 2016, 94, 094417
[35] Yu S, Zhao G Q, Peng Y, et al. A substantial increase of Curie temperature in a new type of diluted magnetic semiconductors via effects of chemical pressure. APL Mater, 2019, 7, 101119

Jinou Dong is a PhD candidate in the Department of Physics, Zhejiang University. Her supervisor is Professor Fanlong Ning, and her main research interests are the preparation and characterization of novel diluted magnetic semiconductors.

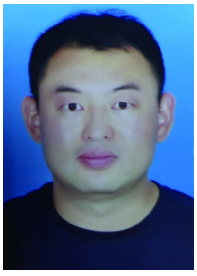

Fanlong Ning works on the synthesis and microscopic characterization of unconventional superconductors and novel magnetic semiconductors. He has published more than 60 papers, which have been cited more than 2300 times. He has given more than 50 invited talks at conferences and workshops.